How to cite: *Angew. Chem. Int. Ed.* **2022,** *61,* e202201565
International Edition: doi.org/10.1002/anie.202201565
German Edition: doi.org/10.1002/ange.202201565

Photopharmacology

BTDAzo: A Photoswitchable TRPC5 Channel Activator**

*Markus Müller, Konstantin Niemeyer, Nicole Urban, Navin K. Ojha, Frank Zufall, Trese Leinders-Zufall, Michael Schaefer, and Oliver Thorn-Seshold**

Abstract: Photoswitchable reagents can be powerful tools for high-precision biological control. TRPC5 is a Ca^{2+}-permeable cation channel with distinct tissue-specific roles, from synaptic function to hormone regulation. Reagents giving spatiotemporally-resolved control over TRPC5 activity may be key to understanding and harnessing its biology. Here we develop the first photoswitchable TRPC5-modulator, **BTDAzo**, to address this goal. **BTDAzo** can photocontrol TRPC5 currents in cell culture, as well as controlling endogenous TRPC5-based neuronal Ca^{2+} responses in mouse brain slices. **BTDAzo**s are also the first reported azobenzothiadiazines, an accessible and conveniently derivatised azoheteroarene with strong two-colour photoswitching. **BTDAzo**'s ability to control TRPC5 across relevant channel biology settings makes it suitable for a range of dynamically reversible photoswitching studies in TRP channel biology, with the aim to decipher the various biological roles of this centrally important ion channel.

Introduction

The twenty-eight Transient Receptor Potential (TRP) channels have crucial roles in sensing and integrating a wide range of stimuli.[1] Better-known members include TRPV1 (heat) and TRPM8 (cold) for which a 2021 Nobel Prize was awarded, and TRPA1 (electrophiles). As these channels are expressed in many tissues but play different biological roles in these tissues,[2] potentially with time-dependent aspects, a range of photoswitchable ligands have been actively developed to elucidate their tissue- and time-specific roles through spatiotemporally precise modulation.[3] Notable photoswitchable TRP ligands include analogues of diacylglycerols (PhoDAGs)[4,5] and of small polar GSK ligands[6] for TRPC2,3,6; azo-vanilloids (azCA4,[7] red-azCA4[8]) for TRPV1; and TRPswitch[9] for TRPA1.

TRPC5 is implicated in a range of tissue-dependent roles in physiology as well as in disease, with brain functions from synaptic plasticity and hormone regulation to potential importance in metabolic medicine.[2,10–12] TRPC1,4 and 5 share substantial structural overlap which drives the typically poor channel selectivity of TRPC1/4/5 ligands; however, drug discovery for TRPC5 has recently yielded a treasure trove of valuable ligands.[13,14] Weak antagonists were first identified from screening,[15] before Christmann, Beech, Waldmann and co-workers identified TRPC5 as one of the targets of the potent but nonselective TRPC4/5-targeting natural product agonist **Englerin A**[16,17] (Figure 1a). Moderately potent synthetic agonist **BTD** was also

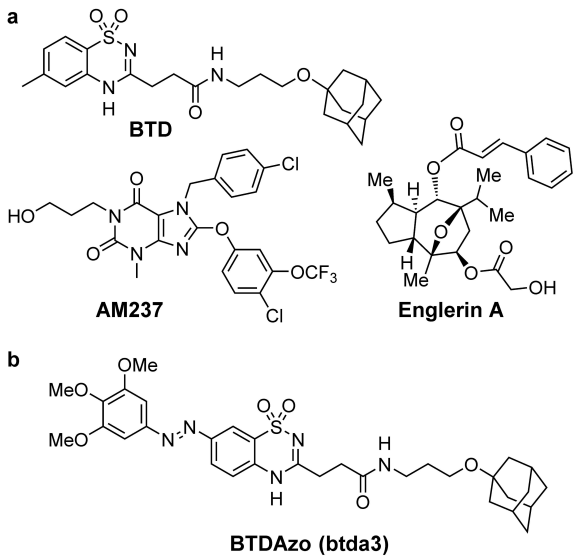

Figure 1. Design (see Supporting Information for high-resolution vectorial copies of all main text Figures). a) Known TRPC5 agonists **BTD**, **Englerin A**, **AM237**. b) **BTDAzo**, the best photoswitchable agonist of the series **btda1**–**btda7** (cf. Figure S1).

[*] M. Müller, Dr. O. Thorn-Seshold
Department of Pharmacy, LMU Munich
Butenandtstrasse 7, 81377 Munich (Germany)
E-mail: oliver.thorn-seshold@cup.lmu.de
K. Niemeyer, N. Urban, Prof. Dr. M. Schaefer
Rudolf-Boehm-Institute of Pharmacology and Toxicology, Leipzig University
Härtelstraße 16–18, 04107 Leipzig (Germany)
Dr. N. K. Ojha, Prof. Dr. F. Zufall, Prof. Dr. T. Leinders-Zufall
Center for Integrative Physiology and Molecular Medicine, Saarland University
Kirrbergerstraße 100, 66421 Homburg (Germany)

[**] A previous version of this manuscript has been deposited on a preprint server (https://doi.org/10.26434/chemrxiv-2022-hvh6b).

identified by Schaefer, with the unusual feature of excellent selectivity for TRPC5 and no activity on TRPC4.[18] Boehringer-Hydra disclosed high-potency xanthine antagonist leads intended to treat anxiety,[19,20] that Muraki, Beech and co-workers characterised as effective TRPC5 modulator tool compounds;[21] Bon, Muraki and co-workers characterised these xanthines further to identify compounds with intriguing selectivity and mixed agonist-antagonist profiles (e.g. **AM237**; Figure 1a)[22] as well as identify the Pico145 binding site.[23,24]

However, no photoswitchable TRPC5 ligands have yet been reported, which could help to study its tissue- and time-resolved biological roles. We therefore wished to create TRPC5-selective photoswitchable ligands, with minimal effects on TRPC1/4 channels, as high spatiotemporal-precision tools with useful biochemical selectivity. **BTD** represented a good basis structure for this goal. Although its potency is moderate (EC_{50} $1.4 \pm 0.3\,\mu M$), it selectively activates homomeric TRPC5 or heteromeric TRPC[1/4/]5 channel complexes that contain TRPC5 subunits, while not activating homomeric TRPC4: making it a more selective tool than e.g. **AM237** or **Englerin A**. We set out to create a photoswitchable analogue of **BTD** for applications in researching the role of endogenous TRPC5 in mammalian cells and tissue slices.

Results and Discussion

Design and Synthesis

The TRPC5 binding mode of **BTD** is unknown, and structure–activity-relationship data are limited (the 4-methyl group on the benzothiadiazine can be deleted, but shorter spacers between the adamantane and benzothiadiazine abolish activity).[18] We tested applying the bidirectional photoswitch azobenzene to the **BTD** scaffold at each end, presuming that one end could be sterically tolerated.

Firstly, we extended the azobenzene from the benzothiadiazine ring, though in *para* to the nitrogen. This was chosen hoping that this unknown azoheteroarene that is electronically similar to a *para*-anilide, could provide similarly desirable photoswitching properties, as are necessary for creating an effective photopharmaceutical: i.e. bidirectional photoswitching with near-UV and blue-green light each achieving high photostationary states (PSSs).[25] We varied the azophenyl substitution pattern to scan for different polarities, PSSs, and $Z \rightarrow E$ spontaneous relaxation rates: comparing unsubstituted, with *para*-methoxy and trimethoxy (improved PSSs), and *para*-hydroxy (faster relaxation) designs **btda1**–**btda4** (Figure S1). Secondly, we replaced the hydrophobic adamantyl group with the azobenzene: retaining the oxyether attachment site because of its beneficial effects on photoswitching,[26] and employing an unsubstituted, *para*-methoxy, or a bulky bis-isopropyl azobenzene to increasingly mimic the hydrophobicity of the adamantyl, in case this (rather than sterics) were the driving force of BTD binding. This yielded designs **btda5**–**btda7** (Figure S1).

The seven candidates **btda1**–**btda7** were assembled over three to six least linear steps, with good yields in all steps for except the final *O*-methylations of **btda2** and **btda3**; representative synthesis of **btda3** is shown in Scheme 1. **btda1**–**btda7** were typically obtained in 10 mg batches and excellent purity, sufficient for biological evaluations (see Supporting Information for details).

Photoswitchability

Pleasingly, the as-yet unstudied phenylazo-benzothiadiazine (**btda1**–**btda4**) proved to be an excellent photoswitch, with performance recalling that of *para*-anilides. As expected for mono/bis-*para*-alkoxy azobenzenes,[26] **btda5**–**btda7** also had high PSS ratios and efficient photoswitching. As **btda3** later gave the best biological performance, it was renamed **BTDAzo**, and studied in detail. Like classical azobenzenes, the *E*-isomer is thermodynamically preferred, and all-*E*

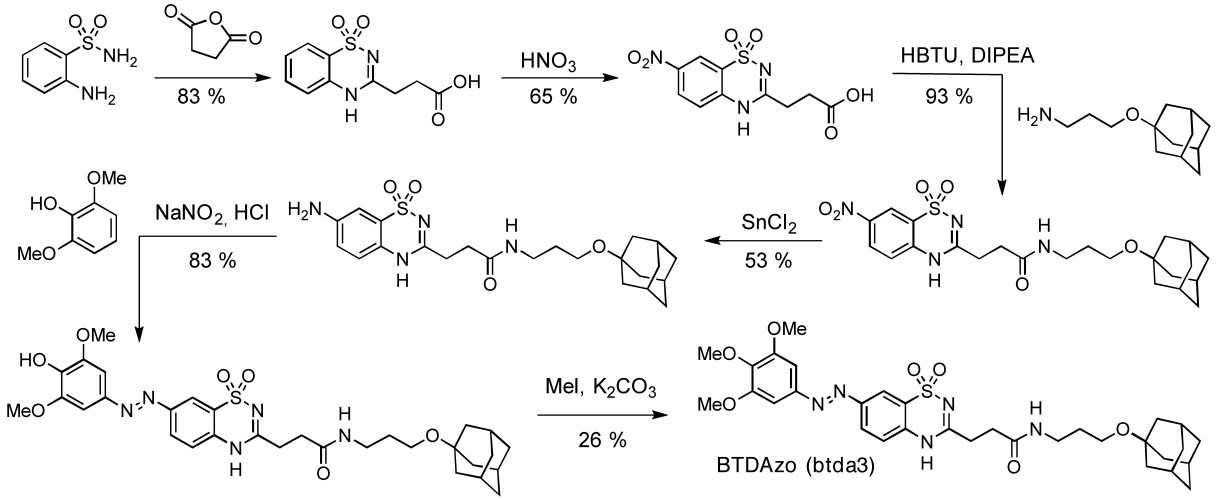

Scheme 1. Synthesis of **BTDAzo** (**btda3**).

populations are reached by maintaining DMSO solution stocks at 60 °C overnight. **BTDAzo** could be reversibly photoswitched between majority-*E* and majority-*Z* populations, reaching solvent-dependent PSSs with up to 94 % *Z* (380 nm) and 87 % *E* (520 nm) in apolar solvents that mimic the expected cellular lipid environment for this hydrophobic compound (Figure 2a–c; Figure S2). The spectral separation between *E* and *Z* bands that results in the *Z* absorption minimum being located at the same wavelength as the *E* absorption maximum (Figure 2d) is the driver of the high-*Z* PSS.

Photoswitching in aqueous media was also strong and was photoreversible over many cycles with no photoinstability noted (Figure 2e). *Z*→*E* thermal relaxation below 40 °C was significantly slower than the timescales of channel switching experiments (Figure S3). PSS spectra and discussions of photochemistry for other **btda** derivatives are given in the Supporting Information in Figures S3 and S4.

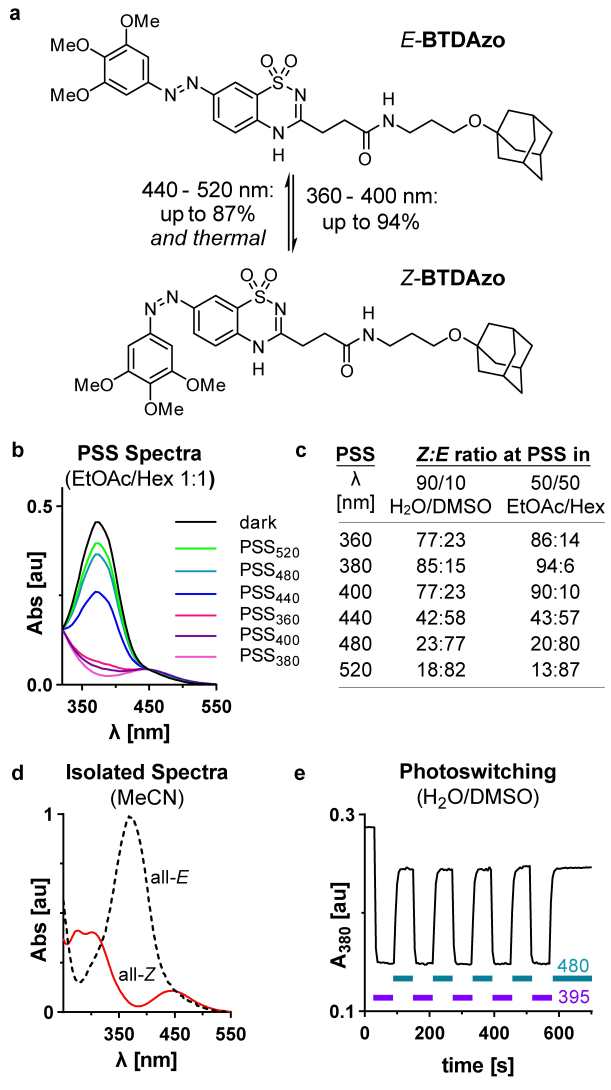

Figure 2. Photocharacterisation. a) *E*⇄*Z* isomerisations of **BTDAzo**. b) *Z*:*E* ratios at PSS depending on environment. c) PSS spectra of **BTDAzo** in H_2O/DMSO. d) Spectra of pure *E*- and *Z*-**BTDAzo** (inline HPLC detection). e) **BTDAzo** can be reversibly photoswitched between PSS states.

Cellular TRPC5 Photopharmacology

We initially screened **btda1**–**btda7** as photoswitchable TRPC5 agonists in cells, using human embryonic kidney cell line HEK293 stably transfected to express a mouse TRPC5-CFP fusion protein ($HEK_{mTRPC5\text{-}CFP}$). $HEK_{mTRPC5\text{-}CFP}$ cell suspensions were loaded with the fluorescent Ca^{2+} indicator dye precursor Fluo-4/AM, washed, and dispensed into black pigmented clear-bottom 384-well microplates to monitor ion channel opening in a custom-made fluorescence imaging plate reader device. By adding serially diluted compounds to single wells, this is a convenient high-throughput method to obtain concentration-response curves before and during controlled application of ultraviolet light to the bottom of the microplate. We wished to use alternating cycles of moderate intensity 360/447 nm light for substantial *E*⇄*Z* photoswitching. The fluorescent Ca^{2+} indicator Fluo-4 was either excited at 447 nm for combined detection and off-switching, or at low intensities at 470 nm to achieve a lower impact on **btda** photostationary states due to the small extinction coefficients in the cyan (Figure S4).

BTDAzo (**bdta3**) was the best hit from this screening: it gave highly repeatable, bidirectional Ca^{2+} influx signals with low basal activity as the relaxed *E* isomer and robust responses upon photoswitching with 365 nm light (Figure 3a). **BTDAzo** showed several outstanding features. Firstly, the potency of *Z*-**BTDAzo** (EC_{50} 1.5 μM for the mostly-*Z* PSS at 365 nm: for simplicity now referred to as "*Z*-potency"; Figure 3b) was as good as that of its parent molecule **BTD** (EC_{50} 1.4 μM);[18] potency matching is only very rarely achieved in photopharmacology.[27] Secondly, not only was all-*E*-**BTDAzo** at 50 μM fully inactive on TRPC5 (Figure 3b), and nearly non-responsive to 470 nm imaging (initial 60 s of Figure 3a), but using 440 nm light to photoswitch 50 μM **BTDAzo** that had previously been in the mostly-*Z*-state reduced channel currents to below those seen with mostly-*Z* **BTDAzo** at just 1.5 μM. **BTDAzo**'s combination of activity exclusively in the *Z*-isomer, with efficient *Z*→*E* photoswitching at 440 nm in cells, helps give it such effective bidirectional *photoswitching of bioactivity*: although the actively antagonistic effect of its *E*-isomer was later identified as a third important factor (see below). Thirdly, no "biological fatigue" was seen, as photoswitching of **BTDAzo** was highly repeatable over many cycles. Thus **BTDAzo** could be a robust tool for complex studies (particularly since, as a lit-active photoswitch, it avoids background bioactivity in non-illuminated cells). The other **btdas** were not good tool compounds: **btda1**,**2**,**4** gave much slower bulk photoresponses, while **btda5**–**btda7** were inactive (see Figure S5 and Supporting Information).

Since the plate imaging device uses single-color light-emitting diodes for Fluo-4 detection as well as for **BTDAzo** photoswitching, no continuous spectral information could be gathered in this assay. We therefore used single-cell Ca^{2+} imaging with a Xenon lamp-equipped monochromator as

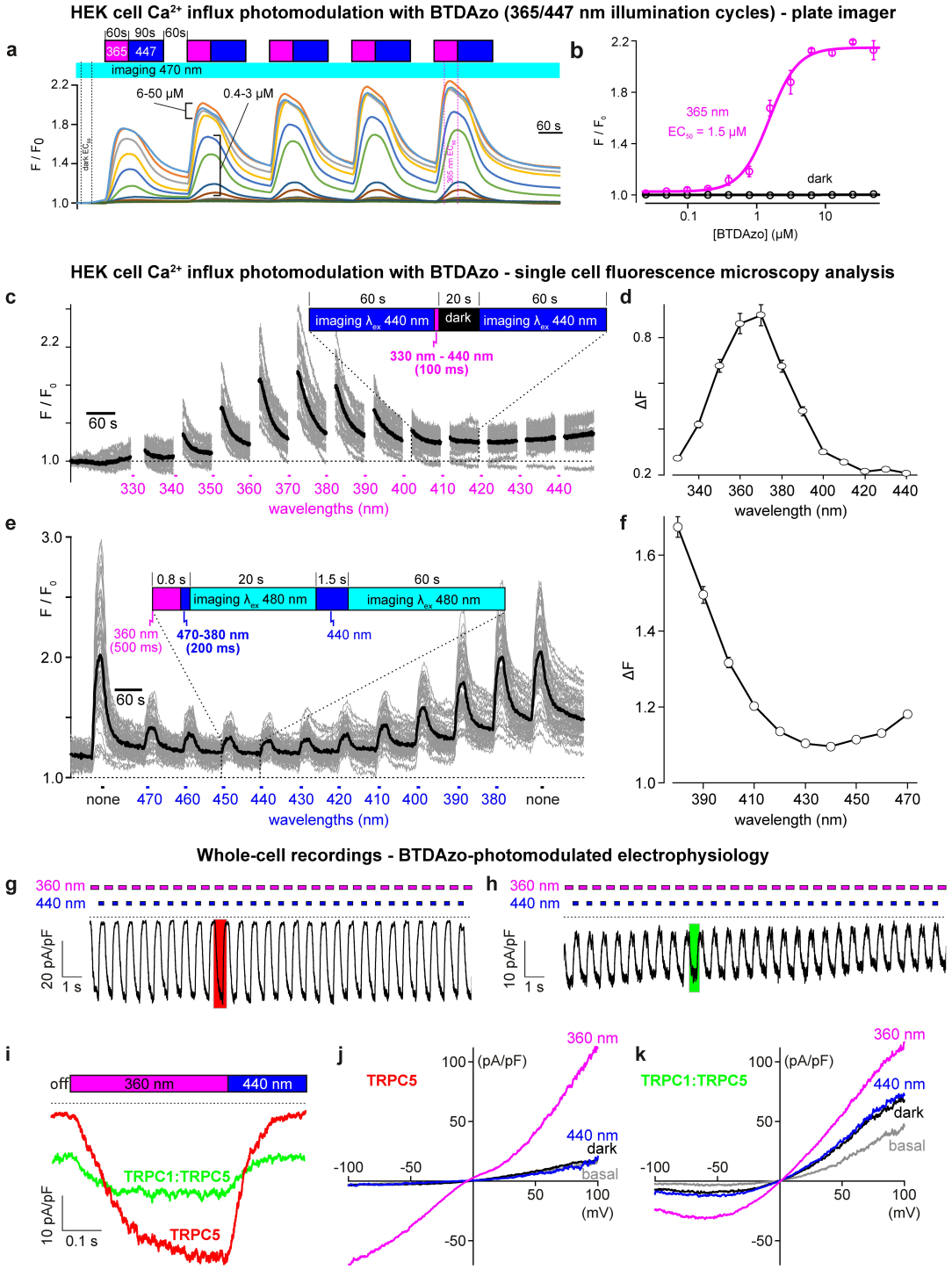

Figure 3. Cellular TRPC5 photoswitching with BTDAzo (see Supporting Information for high-resolution vectorial copies of all main text Figures). a), b) Reversible Ca^{2+} influx modulation with **BTDAzo** under cycles of 365/447 nm illumination, and peak amplitudes (mostly-*Z*-**BTDAzo**), as detected in Fluo-4-loaded $HEK_{mTRPC5\text{-}CFP}$ cell suspensions by fluorescence plate imager (values in b are means ± S.E., averaged over the time periods illustrated between dotted vertical lines in panel a). For additional information see Figure S5. c)–f) Microfluorometric single cell analysis (60 grey traces: single cells; black trace: averaged signal) of TRPC5 activation measured with a monochromator-equipped Xenon light source. c), d) Cellular action spectrum for stimulation of Ca^{2+} influx into single $HEK_{mTRPC5\text{-}CFP}$ cells by *E*→*Z* **BTDAzo** isomerisation. e), f) Cellular action spectrum for preventing Ca^{2+} influx, by *Z*→*E* **BTDAzo** isomerisation at various wavelengths immediately after *E*→*Z* isomerisations. g)–i) Electrophysiological whole-cell recordings of TRPC5 currents in voltage clamp (V_h = -80 mV) mode. g) Ionic currents in a TRPC5-expressing HEK293 cell during 60 consecutive cycles of 360/440 nm illumination in the presence of 10 µM **BTDAzo**. Dotted line shows zero current level (half of each time course shown). h) Ionic currents in TRPC5/TRPC1-co-expressing HEK293 cell, as in panel g. i) Magnification of single on-off cycles taken from the traces shown in (g), (h) as indicated by the coloured boxes. j)–k) *I*/*V* curves of whole cell currents in voltage-clamped TRPC5- or TRPC5/TRPC1-expressing cells exposed to 360 nm and 440 nm light with 10 µM **BTDAzo** in the bath solution. Note the distinct shape of the *I*/*V* curve in panel k, with smaller inward current component. All data from a minimum of 3 independent experiments, each run in technical duplicates.

excitation light source to study the cellular action spectra (channel current dependency on wavelength) and cellular power spectra (channel current dependency on applied photon flux), and to optimise assay illumination protocols. $E \rightarrow Z$ action spectra showed optimal photo-switch-on response to ca. 360–370 nm (Figure 3c, d) when measured in flux-limited conditions designed to minimise photobleaching (power spectrum Figures S6a and S6b). $Z \rightarrow E$ action spectra showed optimal photo-switch-off response to ca. 420–460 nm (Figure 3e, f) in flux-limited conditions (power spectrum Figures S6c and S6d). The striking action spectrum peak sharpness (Figure 3d), and the mismatch between the poor photoswitching completion in homogeneous polar media such as DMSO:water (Figure 1c) and the excellent performance in cells, indicate that cell-free measurements are only approximately predictive of the cellularly-relevant photoswitching of this lipophilic photoswitch (discussions in Supporting Information at Figure S4 [relaxation timescales] and Figure S6 [action spectra]). The power spectra additionally highlight that bulk $E \rightarrow Z$ and $Z \rightarrow E$ photoswitching in the cellular setting proceed at comparable rates (50 % conversion at 30 mJ cm^{-2} for 360 nm and 50 mJ cm^{-2} for 440 nm; Figure S6); this is a reminder that the ratio of E/Z extinction coefficients is more important for photoswitching performance in microscopy, than are their absolute magnitudes (ca. tenfold lower at 440 nm than at 360 nm).

We next performed patch clamp experiments, a non-optical current readout that can orthogonally confirm and characterise the specificity of channel modulation. In the presence of 10 μM **BTDAzo**, on/off-photoswitching of ionic currents in TRPC5-expressing cells was fully reproducible over 60 cycles (Figure 3g) with 360 nm rapidly opening then 440 nm almost fully reclosing channels to baseline conductivity (Figure 3i). The efficient channel closure following 440 nm illumination was seen over the entire current–voltage plot range (Figure 3j).

An interesting question raised by this result is: why are TRPC5 currents so efficiently shut down to baseline by photoswitching at 440 nm (Figure 3g), when photoswitching at this wavelength is not complete (ca. 42 % Z remaining in cell-free tests either in polar protic or apolar aprotic media)? One hypothesis is that the E-isomer which is inactive on the channel (Figure 3b, "dark" curve) binds TRPC5 competitively to the Z-isomer and so prevents channel opening, potentially with complex stoichiometry from the tetrameric nature of the channel. To begin exploring this without the complications of uncertain photostationary states, we competed E-**BTDAzo** against the parent activator **BTD**. We found that it indeed shuts down **BTD**-induced Ca^{2+} currents, providing initial support for this hypothesis (Figure S7).

BTD is a strong tool compound because of its high selectivity for TRPC5-containing channels,[18] while most other TRPC5 ligands also target TRPC4. To begin testing whether **BTDAzo** retains this TRPC5-selectivity, we imaged TRPC4-expressing HEK293 cells in FLIPR, and pleasingly saw no TRPC4-mediated photostimulation of Ca^{2+} influx responses under any of the BTD derivatives applied at concentrations up to 50 μM, including **BTDAzo** (Figure S8). We did not assay and so cannot exclude that TRPC1/C4 channels might be activated by **BTDAzo**, so the selectivity we assess of **BTDAzo** for TRPC5 vs. TRPC4 is based on data for TRPC4:C4 channels only (note however that BTD itself does not activate TRPC1/C4). Patch clamp recordings in TRPC1/TRPC5 co-expressing cells exposed to 10 μM **BTDAzo**, however, showed strong and reversible photocontrol (Figure 3h, i) of inward and outward currents, with a characteristic shape of the I/V curve that is known to result from the assembly of TRPC1 and TRPC5 channel subunits into heteromeric channel complexes (Figure 3k). This finding is reminiscent of the parent compound **BTD**, which also activates heteromeric TRPC1/C5 channel complexes.

Taken together, we conclude that **BTDAzo** is a fully reversible, binary "fully-off⇌fully-on" performing photoswitchable agonist for cellular TRPC5 channels.

Tissue Slice Photopharmacology—Hypothalamic Mouse Dopamine Neurons

We now wished to use **BTDAzo** to probe the role of TRPC5-dependent responses in dopamine (i.e. tyrosine hydroxylase-positive, Th+) neurons of the hypothalamic arcuate nucleus (ARC) (Figure 4a). TRPC5 contributes to both spontaneous oscillatory activity and persistent activation after stimulation with the maternal signalling hormone prolactin[28] making TRPC5 essential for normal prolactin homeostasis of the body (Figure 4a).[11]

We took slices through the ARC of mice expressing the Ca^{2+} indicator GCaMP6f in Th+ neurons (Figure 4b, c) to test whether **BTDAzo** illumination could achieve photocontrol over Ca^{2+} responses at endogenous TRPC5 expression levels. In Th+ neurons, with sparse endogenous expression of TRPC5, long-lasting oscillatory Ca^{2+} signals are seen with delayed onset after prolactin receptor or after direct TRPC5 stimulation. These are a secondary response which is due to Ca^{2+} entry through voltage-gated channels, that are activated after sustained depolarising Na^+ and Ca^{2+} influx through TRPC5; and therefore, the measured Ca^{2+} responses are seen as trains of more frequent and higher-intensity spikes, as compared to baseline.

Spontaneous Ca^{2+} response trains in Th+ neurons after treatment with **BTDAzo** and 355 nm photoactivation matched those upon treatment with either prolactin or **BTD** (Figure 4d, f). Genetic deletion of the TRPC5 channel in the Th-GCaMP6f-ΔTrpc5 mouse prevented the increase in Ca^{2+} activity in Th+ neurons (Figure 4g), indicating the channel selectivity of **BTDAzo** in the slice setting. The area under the curve (AUC) of the Ca^{2+} signals quantifies that **BTDAzo** does not induce changes under 488 nm illumination alone, but needs both isomerisation with 355 nm light *and* TRPC5 expression to generate Ca^{2+} rises ($p < 0.0001$) (Figure 4h, i; Figures S9a–S9c); and the delay time before the increase of Ca^{2+} activity was inversely correlated to the UV photon flux applied, matching expectations for a photocontrolled tool (Figure S9d, e).

Thus, **BTDAzo** can be used in complex tissue slice settings as a highly selective direct activator of the TRPC5

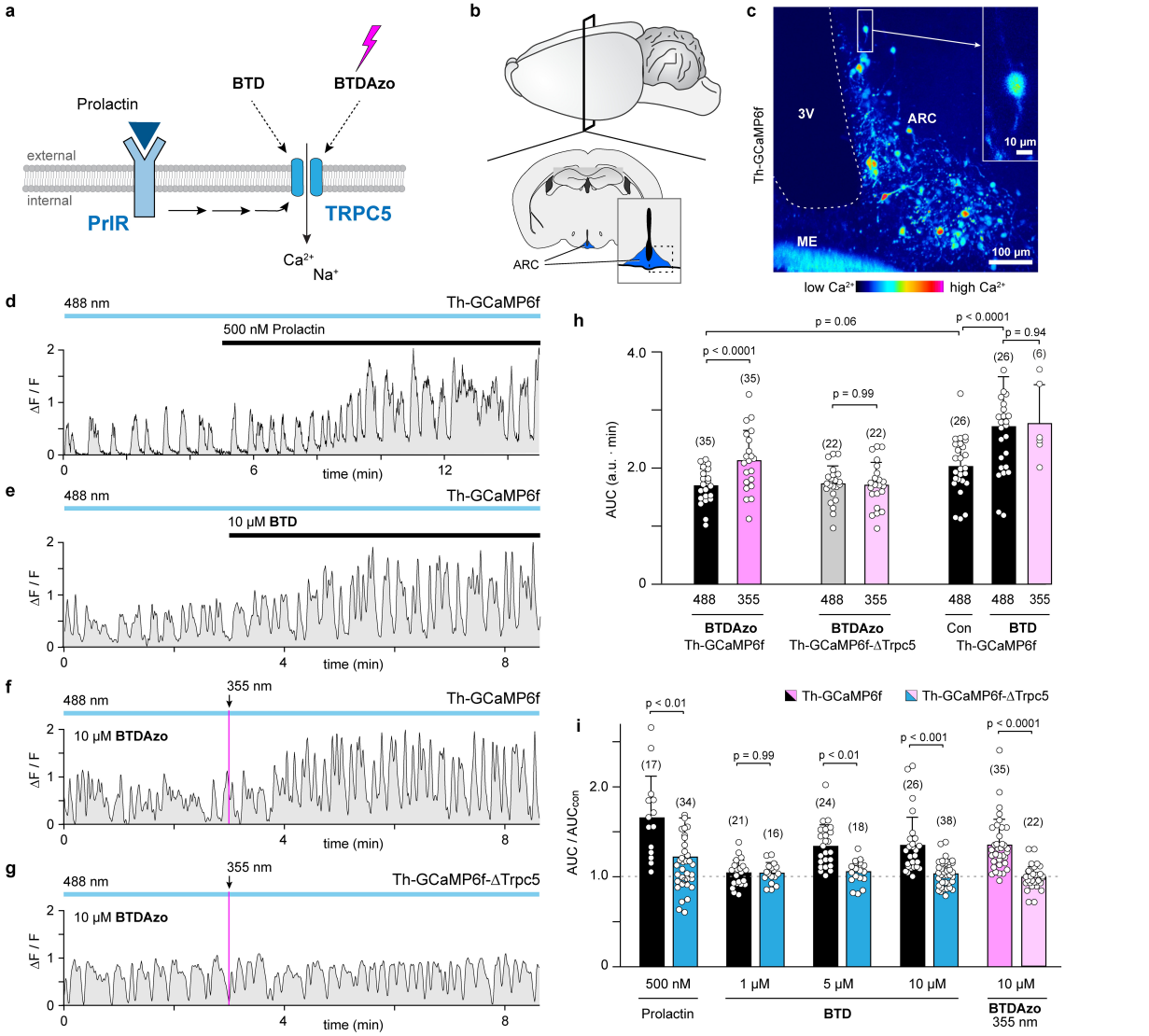

Figure 4. **BTDAzo** photocontrols endogenous TRPC5-dependent Ca^{2+} responses in mouse brain (see also Figure S9). a) Cascade model for TRPC5-dependent cation channel activation in Th+ neurons of the hypothalamic arcuate nucleus (ARC) after stimulation of the prolactin receptor (PrlR). b) Cartoon of the coronal brain slice, and region of the ARC (blue). Dashed box indicates the ARC region in (c). c) Pseudocoloured image of Th+ neurons expressing GCaMP6f in a mouse brain slice. Inset: Zoom on a GCaMP6f neuron from the dorsomedial region of the ARC. (3 V, third ventricle; ME, median eminence). d)–g) Original traces of spontaneous Ca^{2+} responses in Th+ neurons of Th-GCaMP6f mice, stimulated with prolactin (d), **BTD** (e), or **BTDAzo** followed by $E \rightarrow Z$ isomerisation using 355 nm UV laser stimulation (f: total UV exposure time, 14.1 ms; response delay, 48 s). f), g) Panel (g) shows data for the TRPC5-deficient Th+ neuron of Th-GCaMP6f-ΔTrpc5 mouse (total UV exposure time, 14.5 ms). h) Area under the curve (AUC) of Ca^{2+} signals when applying **BTDAzo** under 488 or 355 nm in wildtype or Trpc5 deficient Th+ neurons, compared with wildtype cosolvent only (Con) or **BTD** controls. Two-way ANOVA: $F(3, 158) = 3.011$, $p < 0.05$. i) Wildtype or knockout AUCs normalized to their controls (cosolvent or 488 nm stimulation of BTDAzo) show prolactin, **BTD**, and **BTDAzo** after 355 nm photoswitching stimulate TRPC5-dependent Ca^{2+} increases. Kruskal-Wallis ANOVA: $\chi^2(9) = 95.24$, $p < 0.00001$. [h, i): number of cells is indicated in parentheses above each bar; for full description of material methods and statistics, see Supporting Information.]

channel complex, that acts only upon $E \rightarrow Z$ photoswitching to measurably increase sustained influxes of Ca^{2+} mimicking those seen with the endogenous upstream activating hormone, prolactin.

Conclusion

Photopharmaceuticals are proving to be powerful and flexible tools to non-invasively manipulate and study biological processes, with the high temporal and spatial resolution that is appropriate to their biology.[29,30]

We here report the first photoswitchable ligand for the ion channel TRPC5. **BTDAzo** can reversibly photoswitch cellular channel activity between opened (conducting) and

full baseline states, and its potency and selectivity for TRPC5 against the typical cross-hit channel TRPC4 are additional promising features for future research. Its channel activation is potent enough to be applicable not only in overexpression systems, but in brain tissues with sparse endogenous TRPC5 expression levels, and its pharmaceutical properties make it suitable for tissue slice use. Following the proof-of-concept brain slice assay we have tested, we consider **BTDAzo** as a valuable tool to investigate the various roles of TRPC5 (and so distinguish them from the distinct roles of TRPC4) in brain function, including their potential in the study and treatment of metabolic disease.[12]

We believe this is also the first report of azobenzothiadiazines as photoswitches for cell biology. It can give favourably complete bidirectional photoswitching with rapid response under biologically available wavelengths, and its easy synthesis and handling recommend it for use towards other photopharmaceuticals.

Challenges for the ongoing development and use of TRPC5 photopharmaceuticals in focus in our group include i) improving ligand potency, and ii) improving solubility and bioavailability, which should broaden the scope of applications of these ligands towards real-time in vivo uses.[31] Nevertheless, **BTDAzo** is a reliable, potent TRPC5 photoswitch that can easily find applications in cell culture and slice use towards a better understanding of this truly remarkable protein.

Acknowledgements

We thank the German Research Foundation (DFG: SFB TRR 152 number 239283807 projects P10 to F.Z./T.L.-Z., P18 to MS, P24 to O.T.-S.; Emmy Noether number 400324123 to O.T.-S.) for funding. Open Access funding enabled and organized by Projekt DEAL.

Conflict of Interest

The authors declare no conflict of interest.

Data Availability Statement

The data that support the findings of this study are available from the corresponding author upon reasonable request.

Keywords: Agonists · Cation Channels · Ligand Design · Photopharmacology · Prolactin Signaling

[1] "Mammalian Transient Receptor Potential (TRP) Cation Channels": V. Flockerzi, B. Nilius in *Handbook of Experimental Pharmacology, Vol. 222* (Eds.: B. Nilius, V. Flockerzi), Springer, Berlin, **2014**, pp. 1–12.
[2] S. Sharma, C. R. Hopkins, *J. Med. Chem.* **2019**, *62*, 7589–7602.
[3] S. Curcic, O. Tiapko, K. Groschner, *Pharmacol. Ther.* **2019**, *200*, 13–26.
[4] T. Leinders-Zufall, U. Storch, K. Bleymehl, M. Mederos y Schnitzler, J. A. Frank, D. B. Konrad, D. Trauner, T. Gudermann, F. Zufall, *Cell Chem. Biol.* **2018**, *25*, 215–223.e3.
[5] T. Leinders-Zufall, U. Storch, M. Mederos y Schnitzler, N. K. Ojha, K. Koike, T. Gudermann, F. Zufall, *STAR Protocols* **2021**, *2*, 100527.
[6] O. Tiapko, N. Shrestha, S. Lindinger, G. G. de la Cruz, A. Graziani, C. Klec, C. Butorac, W. F. Graier, H. Kubista, M. Freichel, L. Birnbaumer, C. Romanin, T. Glasnov, K. Groschner, *Chem. Sci.* **2019**, *10*, 2837–2842.
[7] J. A. Frank, M. Moroni, R. Moshourab, M. Sumser, G. R. Lewin, D. Trauner, *Nat. Commun.* **2015**, *6*, 7118.
[8] D. B. Konrad, J. A. Frank, D. Trauner, *Chem. Eur. J.* **2016**, *22*, 4364–4368.
[9] P.-Y. Lam, A. R. Thawani, E. Balderas, A. J. P. White, D. Chaudhuri, M. J. Fuchter, R. T. Peterson, *J. Am. Chem. Soc.* **2020**, *142*, 17457–17468.
[10] "Mammalian Transient Receptor Potential (TRP) Cation Channels": A. V. Zholos, in *Handbook of Experimental Pharmacology, Vol. 222* (Eds.: B. Nilius, V. Flockerzi), Springer, Berlin, **2014**, pp. 129–156.
[11] T. Blum, A. Moreno-Pérez, M. Pyrski, B. Bufe, A. Arifovic, P. Weissgerber, M. Freichel, F. Zufall, T. Leinders-Zufall, *Proc. Natl. Acad. Sci. USA* **2019**, *116*, 15236–15243.
[12] R. S. Bon, D. J. Wright, D. J. Beech, P. Sukumar, *Annu. Rev. Pharmacol. Toxicol.* **2022**, *62*, 427–446.
[13] A. Minard, C. C. Bauer, D. J. Wright, H. N. Rubaiy, K. Muraki, D. J. Beech, R. S. Bon, *Cells* **2018**, *7*, 52.
[14] H. N. Rubaiy, *Br. J. Pharmacol.* **2019**, *176*, 832–846.
[15] J. M. Richter, M. Schaefer, K. Hill, *Mol. Pharmacol.* **2014**, *86*, 514–521.
[16] Y. Akbulut, H. J. Gaunt, K. Muraki, M. J. Ludlow, M. S. Amer, A. Bruns, N. S. Vasudev, L. Radtke, M. Willot, S. Hahn, T. Seitz, S. Ziegler, M. Christmann, D. J. Beech, H. Waldmann, *Angew. Chem. Int. Ed.* **2015**, *54*, 3787–3791; *Angew. Chem.* **2015**, *127*, 3858–3862.
[17] M. J. Ludlow, H. J. Gaunt, H. N. Rubaiy, K. E. Musialowski, N. M. Blythe, N. S. Vasudev, K. Muraki, D. J. Beech, *J. Biol. Chem.* **2017**, *292*, 723–731.
[18] H. Beckmann, J. Richter, K. Hill, N. Urban, H. Lemoine, M. Schaefer, *Cell Calcium* **2017**, *66*, 10–18.
[19] S. Just, B. L. Chenard, A. Ceci, T. Strassmaier, J. A. Chong, N. T. Blair, R. J. Gallaschun, D. del Camino, S. Cantin, M. D'Amours, C. Eickmeier, C. M. Fanger, C. Hecker, D. P. Hessler, B. Hengerer, K. S. Kroker, S. Malekiani, R. Mihalek, J. McLaughlin, G. Rast, J. Witek, A. Sauer, C. R. Pryce, M. M. Moran, *PLoS One* **2018**, *13*, e0191225.
[20] "Substituted Xanthines and Methods of Use Thereof": B. L. Chenard, R. J. Gallaschun, WO2014143799A3, **2014**.
[21] H. N. Rubaiy, M. J. Ludlow, M. Henrot, H. J. Gaunt, K. Miteva, S. Y. Cheung, Y. Tanahashi, N. Hamzah, K. E. Musialowski, N. M. Blythe, H. L. Appleby, M. A. Bailey, L. McKeown, R. Taylor, R. Foster, H. Waldmann, P. Nussbaumer, M. Christmann, R. S. Bon, K. Muraki, D. J. Beech, *J. Biol. Chem.* **2017**, *292*, 8158–8173.
[22] A. Minard, C. C. Bauer, E. Chuntharpursat-Bon, I. B. Pickles, D. J. Wright, M. J. Ludlow, M. P. Burnham, S. L. Warriner, D. J. Beech, K. Muraki, R. S. Bon, *Br. J. Pharmacol.* **2019**, *176*, 3924–3938.
[23] D. J. Wright, K. J. Simmons, R. M. Johnson, D. J. Beech, S. P. Muench, R. S. Bon, *Commun. Biol.* **2020**, *3*, 704.
[24] C. C. Bauer, A. Minard, I. B. Pickles, K. J. Simmons, E. Chuntharpursat-Bon, M. P. Burnham, N. Kapur, D. J. Beech, S. P. Muench, M. H. Wright, S. L. Warriner, R. S. Bon, *RSC Chem. Biol.* **2020**, *1*, 436–448.
[25] V. A. Gutzeit, A. Acosta-Ruiz, H. Munguba, S. Häfner, A. Landra-Willm, B. Mathes, J. Mony, D. Yarotski, K. Börjesson,

C. Liston, G. Sandoz, J. Levitz, J. Broichhagen, *Cell Chem. Biol.* **2021**, *28*, 1648–1663.
[26] M. Borowiak, W. Nahaboo, M. Reynders, K. Nekolla, P. Jalinot, J. Hasserodt, M. Rehberg, M. Delattre, S. Zahler, A. Vollmar, D. Trauner, O. Thorn-Seshold, *Cell* **2015**, *162*, 403–411.
[27] O. Thorn-Seshold, J. C. M. Meiring in *Microtubules: Methods and Protocols* (Ed.: H. Inaba), Springer US, New York, **2022**, pp. 403–430.
[28] A. Costa-Brito, I. Gonçalves, Cecília R. A. Santos, *Neural Regen. Res.* **2022**, *17*, 1695–1702.
[29] J. Broichhagen, J. A. Frank, D. Trauner, *Acc. Chem. Res.* **2015**, *48*, 1947–1960.
[30] M. J. Fuchter, *J. Med. Chem.* **2020**, *63*, 11436–11447.
[31] X. Gómez-Santacana, S. Pittolo, X. Rovira, M. Lopez, C. Zussy, J. A. R. Dalton, A. Faucherre, C. Jopling, J.-P. Pin, F. Ciruela, C. Goudet, J. Giraldo, P. Gorostiza, A. Llebaria, *ACS Cent. Sci.* **2017**, *3*, 81–91.

Manuscript received: January 28, 2022
Accepted manuscript online: June 17, 2022
Version of record online: July 27, 2022